

Article

Effect of Annealing Temperature on the Mechanical and Corrosion Behavior of a Newly Developed Novel Lean Duplex Stainless Steel

Yanjun Guo ¹, Jincheng Hu ², Jin Li ^{1,*}, Laizhu Jiang ², Tianwei Liu ³ and Yanping Wu ⁴

¹ Department of Materials Science, Fudan University, No. 220, Handan Road, Shanghai 200433, China; E-Mail: 13110300027@fudan.edu.cn

² Research and Development Center, Baosteel Co., Ltd., No. 885, Fujin Road, Shanghai 201900, China; E-Mails: hujincheng@baosteel.com (J.H.); lzjiang@baosteel.com (L.J.)

³ Science and Technology on Surface Physics and Chemistry Laboratory, P.O. Box 718-35, Mianyang 621907, Sichuan Province, China; E-Mail: liutianwei@caep.cn

⁴ China Academy of Engineering Physics, P.O. Box 919-71, Mianyang 621900, Sichuan Province, China; E-Mail: wuyanping@caep.cn

* Author to whom correspondence should be addressed; E-Mail: jinli@fudan.edu.cn; Tel./Fax: +86-21-6564-3648.

Received: 4 May 2014; in revised form: 27 August 2014 / Accepted: 29 August 2014 /

Published: 12 September 2014

Abstract: The effect of annealing temperature (1000–1150 °C) on the microstructure evolution, mechanical properties, and pitting corrosion behavior of a newly developed novel lean duplex stainless steel with 20.53Cr-3.45Mn-2.08Ni-0.17N-0.31Mo was studied by means of optical metallographic microscopy (OMM), scanning electron microscopy (SEM), magnetic force microscopy (MFM), scanning Kelvin probe force microscopy (SKPFM), energy dispersive X-ray spectroscopy (EDS), uniaxial tensile tests (UTT), and potentiostatic critical pitting temperature (CPT). The results showed that tensile and yield strength, as well as the pitting corrosion resistance, could be degraded with annealing temperature increasing from 1000 up to 1150 °C. Meanwhile, the elongation at break reached the maximum of 52.7% after annealing at 1050 °C due to the effect of martensite transformation induced plasticity (TRIP). The localized pitting attack preferentially occurred at ferrite phase, indicating that the ferrite phase had inferior pitting corrosion resistance as compared to the austenite phase. With increasing annealing temperature, the pitting resistance equivalent number (PREN) of ferrite phase dropped, while that of the austenite phase rose. Additionally, it was found that ferrite possessed a lower Volta potential

than austenite phase. Moreover, the Volta potential difference between ferrite and austenite increased with the annealing temperature, which was well consistent with the difference of PREN.

Keywords: lean duplex stainless steel; annealing temperature; mechanical properties; TRIP effect; pitting corrosion behavior; PREN; Volta potential

1. Introduction

Duplex stainless steels (DSSs), strongly relying on a balanced two-phase microstructure of ferrite (α) and austenite (γ), have attractive mechanical and corrosion properties and are thus widely used in the chemical, petrochemical, nuclear, marine and paper industries [1–4]. In past years, the development of DSSs has followed two routes. On one side, great efforts have been made to improve the corrosion resistance of DSSs by increasing the content of chromium (Cr), molybdenum (Mo) and nitrogen (N), e.g., the DSS UNS S32750 with high mass fractions of 25%–27% Cr, 3%–4.5% Mo and 0.25%–0.28% N, which has been developed to meet with the requirement of good resistance and high strength in severe service environment [5–7]. On the other side, in order to conserve resources, “lean” route DSSs, e.g., UNS S32101 type with less nickel (Ni) but higher yield strength and better pitting resistance than standard austenitic grades, have been developed to meet the demand for grades with a lower cost [8–12]. However, the elongation of commercial UNS S32101 was around 30%, which limited the application of lean DSSs in many fields [8,13,14].

Recently, some developed lean DSSs with martensitic transformation have been designed to bring transformation induced plasticity (TRIP) effect and improve the ductility of lean DSSs. Herrera has designed a novel Mn based ductile lean duplex stainless TRIP steel (Fe-19.9Cr-0.42Ni-0.16N-4.79Mn-0.11C-0.46Cu-0.35Si, wt%), which had 1 GPa ultimate tensile strength and an elongation to fracture of above 60% resulted from a sequential martensite transformation of $\gamma \rightarrow \epsilon \rightarrow \alpha'$ [14]. Choi has reported the effects of nitrogen addition on the strain-induced martensitic transformation of Fe-20Cr-5Mn-0.2Ni duplex stainless steel and found that the elongation was up to 60% in some lean DSSs containing 0.3% N [15]. In our work, a new lean duplex stainless steel with a composition of 20.53Cr-3.45Mn-2.08Ni-0.17N-0.31Mo has been developed. With a low Ni content, this resource-saving DSS can be less affected by price fluctuation of precious metal and reduce the risk of both production and uses. Additionally, the elongation has been improved to around 50% thanks to martensitic TRIP effect, which is obviously higher than that of 30% in S32101. Thus, this newly developed DSS holds a great potential to be the promising replacement of UNS S32101 in the advantage of improved properties.

In order to expand the application of this newly developed DSS used in this work, it is of great importance to obtain the suitable mechanical properties and good corrosion resistance. Solution heat treatment shows great impact to the mechanical and corrosion properties of DSS. The aim of the present work is to find the optimum solution heating temperature for the studied specimen based on investigating the relationship between the solution heating temperature and the corresponding mechanical properties and pitting corrosion resistance. The effect of annealing temperature on the

microstructure, mechanical properties and corrosion behavior of this novel lean duplex stainless steel has been characterized by microscope, mechanical test and electrochemical technique.

2. Experimental Section

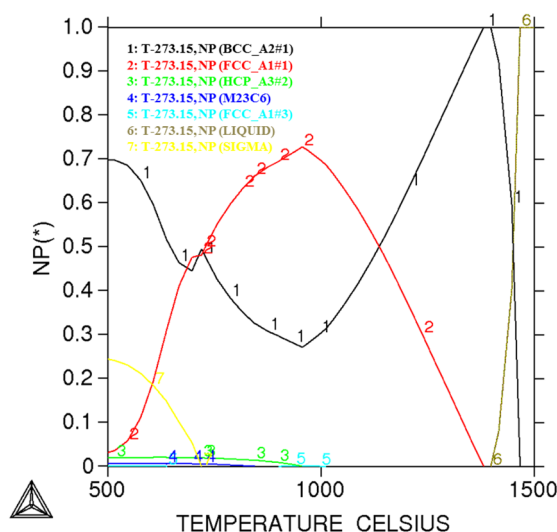
2.1. Materials

The studied material in the paper was a novel developed lean duplex stainless steel with the chemical composition shown in Table 1. It was melted in a 50 kg vacuum furnace and then cast as a single square ingot. After removing the oxide skin, the ingot was forged into square slabs at the temperature ranging from 900 to 1200 °C with a thickness of 40 mm. The slabs were reheated at 1200 °C for 2 h and hot-rolled, using a laboratory hot-rolling mill, into 4 mm thick plates and then cold-rolled into 1.5 mm. The specimens were machined into blocks of dimension of 10 mm × 10 mm. The phase diagram of the newly developed DSS used in present work was calculated by using the Thermo-calc software, as shown in Figure 1. It could be seen that mainly ferrite and austenite were formed in the temperature range between 1000 and 1200 °C. Moreover, the specimen aged between 500 and 980 °C was subjected to precipitation of secondary phases, such as Cr₂N, σ and secondary austenite (γ_2), which would seriously deteriorate the corrosion resistance of the duplex stainless steel [16,17]. Therefore, in the present work, the solution heating temperature below 1000 °C was not chosen so as to avoid the formation of these detrimental secondary phases. Thus, the specimens were subjected to different annealing treatment at 1000, 1020, 1050, 1080, 1110, and 1150 °C for 30 min, respectively, and quenched in water to avoid intermetallic precipitates.

Table 1. Chemical composition (wt%) of the duplex stainless steels (DSS).

UNS No.	C	Si	Mn	P	S	Cr	Ni	Mo	Cu	N
S32750	≤0.03	≤0.8	≤1.2	≤0.035	≤0.02	24.0/26.0	6.0/8.0	3.0/5.0	≤0.5	0.24/0.32
S32101	<0.04	<1.0	4.0/6.0	<0.04	<0.03	21.0/22.0	1.35/1.70	0.10/0.80	0.10/0.80	0.20/0.25
New DSS	0.03	0.32	3.45	0.01	0.004	20.53	2.08	0.31	0.34	0.17

Figure 1. The phase diagram calculated by using the Thermo-Calc software for the newly developed DSS used in the present work.



2.2. Uniaxial Tensile Test

The uniaxial tensile tests were conducted at room temperature with specimens having a gage thickness of 1.5 mm and width of 20 mm annealed at different temperatures using an Instron 5985 (Instron company, Pittsburgh, PA, USA) testing machine according to BS EN ISO 6892-1:2009 [18]. The test was carried out at an extension rate of 3 mm/min before reaching yield point and 20 mm/min after reaching yield point. The test was conducted with three parallel specimens for every annealing temperature and the average data were used for determination of the tensile strength, yield strength and elongation at break values in this paper. In order to observe the microstructure of annealed specimens, which were pre-stretched to 40%, the specimens were etched in 2% HF solution for 30 s, to make the ferrite, austenite, and martensite be distinguished in the optical images.

2.3. Electrochemical Measurement

Electrochemical corrosion behavior of the specimens were performed with a CHI 660D potentiostat (Shanghai Chenhua Instrument Co., Ltd, Shanghai, China). All the measurements were carried out with a three-electrode cell where a Pt foil acted as the counter electrode and a saturated calomel electrode (SCE) as the reference electrode. The specimens acting as working electrodes were sealed in epoxy resin. Prior to each experiment, the working electrode was wet mechanically ground, subsequently polished with a 1.5 μm diamond paste, ultrasonically cleaned in ethanol and distilled water, and then dried in air. To avoid the crevice corrosion, interfaces between specimen and resin were sealed with silica gel sealant, and dried in air. The exposed electrode surface area was 100 mm^2 . The test solution was 500 mL of 1 mol/L NaCl. According to ASTM G 150-99 (2010) [19], critical pitting temperature (CPT) determination of this novel lean duplex stainless steel was performed via potentiostatic measurements by applying a constant potential of 250 mV SCE and increasing the solution temperature at a rate of 1 $^{\circ}\text{C}/\text{min}$ from 2 $^{\circ}\text{C}$. The CPT was defined as the temperature at which the current sharply increased to 100 μA . After testing, specimens were electrochemically etched for 8 s in 30 wt% KOH solution at applied voltage of 2 V, to make the ferrite and austenite be distinguished in the optical images, and then examined for pits [20]. The CPT measurements of the same specimen for every annealing temperature were repeated at least six times, and the typical data were chosen as the CPT values in this work.

2.4. Optical Metallographic Microscopy and SEM-EDS Analysis

Microstructural examination of specimens after the electrochemical measurements was conducted using optical metallographic microscopy and SEM (SCE Phillips XL30 FEG, Amsterdam, The Netherlands). The volume fraction of ferrite and austenite was evaluated by quantitative metallography based on the software attached to the microscope. Energy dispersive X-ray spectroscopy (EDS) was performed on the individual phases to obtain their elemental composition. Because of the insensitivity of EDS techniques to N, an approximate calculation was conducted to determine the N fraction in both phases. The level of N in ferrite phase was assumed to be the saturation value (around 0.05%) and that of austenite was calculated based on the content of N in the whole alloy and the phase volume fraction [21].

The SEM-EDS analysis was tested with six parallel specimens for every annealing temperature. Each value of the element distribution in Table 2 was an average of more than ten measurements.

Table 2. Chemical composition and pitting resistance equivalent number (PREN) of the two phases for specimens annealed at different temperatures, obtained by EDS.

Annealing temperature	Phase	Volume fraction (%)	Cr (%)	Ni (%)	Mo (%)	N (%)	PREN ₁₆	PREN ₃₀
1000 °C	Ferrite	52.1	21.59	1.51	0.40	0.05	23.710	24.410
	Austenite	47.9	19.37	2.70	0.21	0.30	24.863	29.063
1020 °C	Ferrite	57.9	21.45	1.68	0.32	0.05	23.306	24.006
	Austenite	42.1	19.27	2.62	0.29	0.34	25.667	30.427
1050 °C	Ferrite	61.4	21.24	1.72	0.33	0.05	23.129	23.829
	Austenite	38.6	19.40	2.66	0.28	0.36	26.084	31.124
1080 °C	Ferrite	62.9	21.25	1.52	0.32	0.05	23.106	23.806
	Austenite	37.1	19.31	3.03	0.30	0.37	26.220	31.400
1110 °C	Ferrite	66.2	21.15	1.73	0.35	0.05	23.105	23.805
	Austenite	33.8	19.32	2.77	0.22	0.41	26.606	32.346
1150 °C	Ferrite	69.1	21.05	1.85	0.32	0.05	22.906	23.606
	Austenite	30.9	19.37	2.60	0.29	0.44	27.367	33.527

2.5. Magnetic Force Microscopy (MFM) and Scanning Kelvin Probe Force Microscopy (SKPFM) Measurements

The MFM and SKPFM measurements were performed using a dimension Nanoscope V (Bruker Corporation, Santa Barbara, CA, USA). All measurements were conducted in air at room temperature and an ambient relative humidity of about 45%. The probes used in MFM measurements were Nanoprobe™ (Bruker Corporation, Santa Barbara, CA, USA) MSEP Co/Cr-coated tips with force constant of 2.8 N/m and resonant frequency of 75 kHz, while the probes in SKPFM measurements were SCM-PIT conductive Pt/Ir-coated tips with the same force constant and resonant frequency. A dual-scan mode was used to record a second signal in addition to surface topography signal in MFM and SKPFM measurements. The topography of the sample surface was obtained in the first scan with the tapping mode. In the second scan, the cantilever was lifted up 100 nm to avoid the influence of topographic features. The principle and details of the SKPFM measurement have been reported previously [22,23].

3. Results and Discussion

3.1. Microstructures and Elements Distribution

Figure 2 showed the microstructure of specimens annealed at different temperatures for 30 min. The island-shaped austenite phase was evenly embedded in the band-shaped ferrite matrix. Figure 3 displayed the volume fraction of the ferrite/austenite phases against annealing temperature. It could be observed that as the annealing temperature ranged from 1000 to 1150 °C, the ferrite region gradually increased and austenite region decreased, which was a typical diffusion-controlled solid-state

phase transformation: $\gamma \rightarrow \alpha$ and determined by the equilibrium phase diagram [24]. Besides, the ferrite and austenite phase approximately reached balanced when annealed at 1000 °C (*i.e.*, $\text{Volume}_{\text{Ferrite}}:\text{Volume}_{\text{Austenite}} \approx 1:1$). However, Figure 1 revealed that the equal volume fraction of the two phases in the investigated specimens was achieved at annealing temperature higher than 1000 °C, which was attributed to the fact that the Thermo-Calc described thermodynamic equilibrium conditions while the steels could never be in true equilibrium [10]. The content of main alloying elements measured by EDX in austenite and ferrite phases was listed in Table 2. It was shown that alloying elements, such as Cr and Mo, were enriched in the ferrite phase, while N and Ni were concentrated in the austenite phase. As the annealing temperature was increased, content of Cr and Mo decreased in the ferrite phase, while the content of Cr and Mo in austenite increased slightly. It could be explained by that the higher annealing temperature, resulted in the higher volume fraction of ferrite, which further led that corresponding Cr and Mo were spread over a larger region and diluted [20].

Figure 2. Optical micrographs of specimens annealed at different temperature for 30 min, the dark area representing ferrite while the light representing austenite. (a) 1000 °C; (b) 1020 °C; (c) 1050 °C; (d) 1080 °C; (e) 1110 °C; (f) 1150 °C.

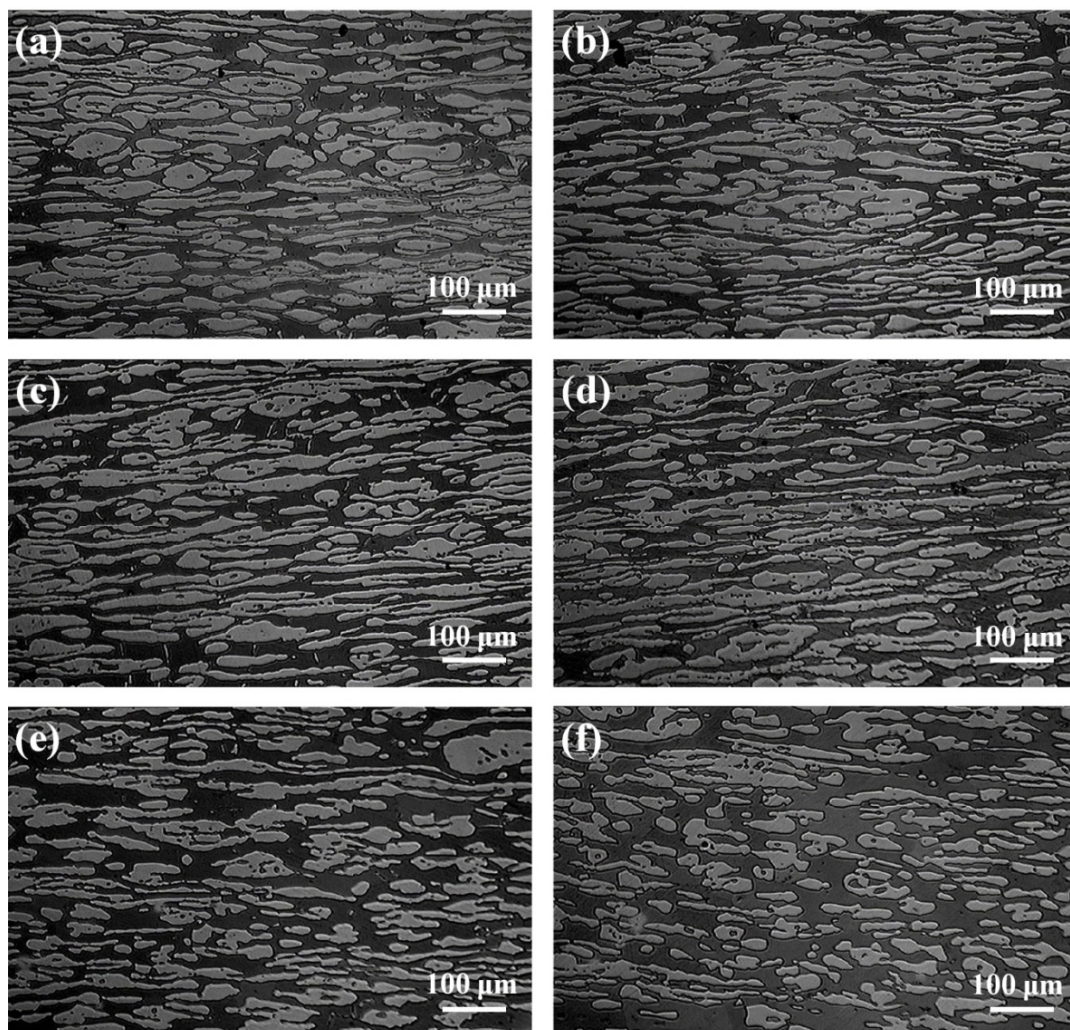
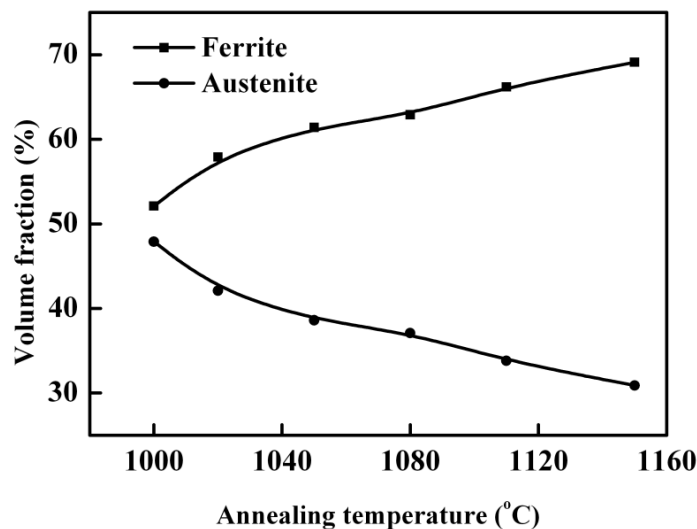


Figure 3. Volume fraction of ferrite and austenite phase with different annealing temperatures for 30 min.



3.2. Mechanical Properties

Figures 4 and 5, respectively, presented the tensile and yield strength of this novel lean duplex stainless steel as function of annealing temperature. The results showed that the tensile strength and yield strength decreased with increasing the annealing temperature from 1000 to 1150 °C. It was revealed that at 1000 °C, the specimens owned the highest tensile and yield strength, which could be attributed to the fact that the tensile and yield strength depended strongly on grain size [2,25,26]. According to the well-known Hall-Petch relation, a smaller average grain size resulted in a stronger material [27]. As the annealing temperature was increased from 1000 up to 1150 °C, the grain growth could be enhanced leading to the increased grain size, thus, the tensile and yield strength decreased. In addition, additional strengthening in DSSs could be caused by solid solution hardening [2]. The solid solution strengthening effects of chromium, molybdenum and nitrogen reached the maximum at 1000 °C as shown by the increased additions of alloying elements in Table 2. Figure 6 showed the elongation at break of this novel lean duplex stainless steel as function of annealing temperature. The elongation at break reached the maximum of 52.7% after annealing at 1050 °C and the minimum of 47.3% at annealing temperature of 1150 °C, being obviously higher than that of 25% in S32750 and 30% in S32101, which might be attributed to the martensite transformation [1,8,13,14,]. Typical values of mechanical properties of solution annealed DSS were summarized in Table 3. The microstructure of specimen annealed at 1050 °C and pre-stretched to 40% is shown in Figure 7. It could be found that much lath-shaped martensite was embedded in dark retained austenite phase, which exhibited that austenite gradually transformed into martensite during tensile deformation. Moreover, it was already demonstrated that the strain-induced martensite transformation was helpful for improving the plasticity of the lean DSS associated with TRIP effect [15]. Meantime, it has been reported that the martensite transformation of lean DSS proceeded from austenite to hexagonal martensite to near cubic martensite ($\gamma \rightarrow \epsilon \rightarrow \alpha'$) [13,14]. However, Zhang has indicated that the main reason for the improvement of elongation of lean DSS was the $\gamma \rightarrow \epsilon$ transformation, not in proportion to the generation of the α' martensite [14]. For this novel lean DSS, the martensite transformation process remained to be

investigated in detail. The elongation at break of specimen annealed at 1000 °C reached 51.13%, which was slightly lower than that of specimen after annealing at 1050 °C. However, combining the tensile and yield strength, the specimen annealed at 1000 °C demonstrated the best mechanical properties.

Figure 4. Tensile strength of specimens with different annealing temperatures for 30 min.

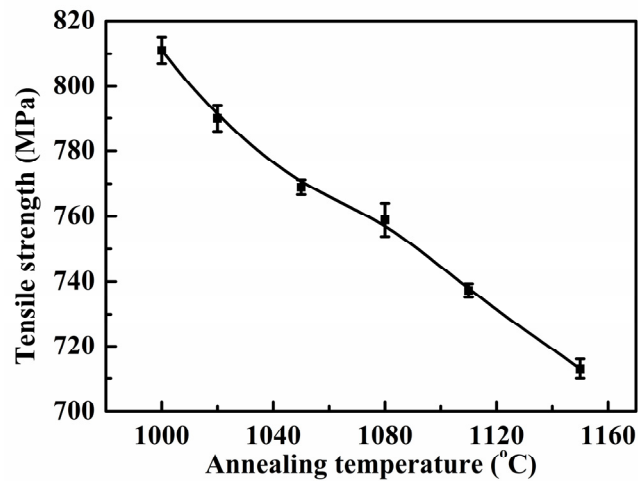


Figure 5. Yield strength of specimens with different annealing temperatures for 30 min.

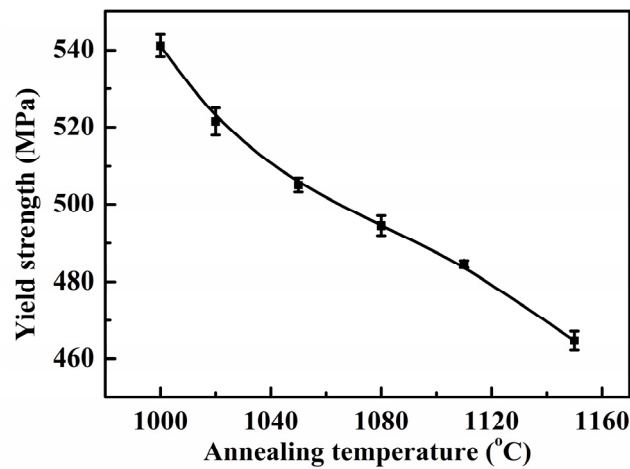


Figure 6. Elongation at break of specimens with different annealing temperatures for 30 min.

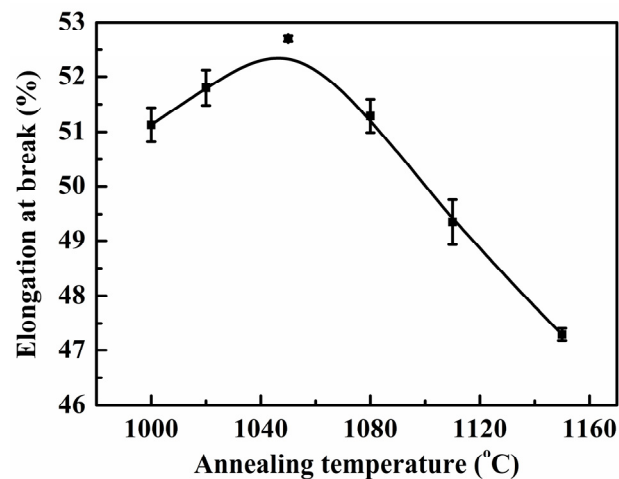
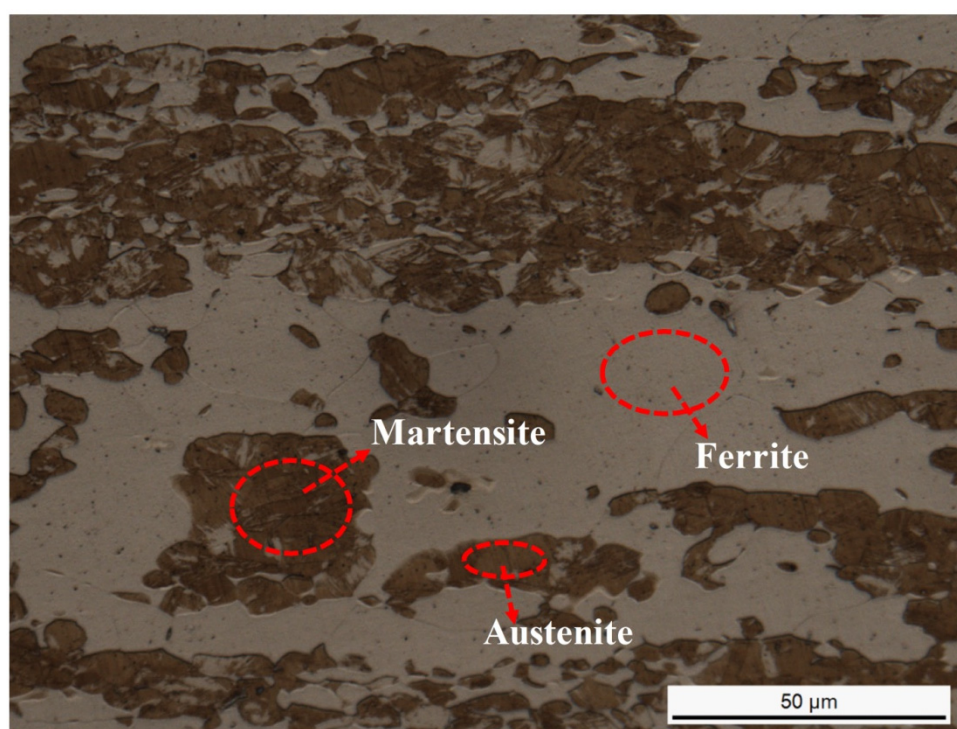


Table 3. Typical values of mechanical properties of solution annealed duplex stainless steels (DSS).

Alloy	Ultimate tensile strength, MPa	0.2% proof stress (min) MPa	Elongation (min) A5, %
UNS S32750 [1]	800–1000	550	25
UNS S32101 [8]	650–700	450	30
Newly Developed DSS	737–811	465	47.3

Figure 7. Optical micrographs of specimen annealed at 1050 °C for 30 min and pre-stretched to 40%, the dark area representing austenite while the light representing ferrite, and lath-shaped martensite was embedded in austenite phase.



3.3. Pitting Corrosion Behavior

Figure 8 illustrated the typical curves of current density against annealing temperature for specimens annealed at different temperatures for 30 min. The current density presented a lower value less than $1 \mu\text{A}/\text{cm}^2$ during the initial heating, indicating that the steel surface was protected by the passive film. With the solution temperature increasing to CPT, some current density fluctuations were found, which were associated with a passive film breakdown in the form of metastable pits. As the temperature increased further reaching to the CPT, the current density rose sharply due to the occurrence of the stable pits. As the annealing temperature increased from 1000 to 1150 °C, the CPT decreased from 40.8 to 27 °C. The highest CPT, 40.8 °C, was obtained when the specimens were annealed at 1000 °C, which meant that the specimens annealed at 1000 °C showed the best pitting corrosion resistance. Compared with the lean duplex stainless steel UNS S32101, of which the highest CPT of 35.2 °C was obtained at annealing temperature of 1000 °C, this novel lean duplex stainless

steel showed a better pitting corrosion resistance [10]. This could be explained by that this novel steel had higher content of N and lower content of Manganese (Mn) than S32101 [28].

The morphologies of specimens were observed under SEM after electrochemical test and stable pits could be found. The stable pitting of specimens annealed at 1000 °C was located at both ferrite phase and austenite phase, while those of specimens annealed at temperatures over 1000 °C mainly distributed from both two phases to ferrite phase and the pitting corrosion occurred randomly. Especially for specimens annealed at 1150 °C, the stable pitting sites mainly attributed in the ferrite phase, and the pitting corrosion preferentially occurred in the ferrite phase. Typical stable pitting morphologies of the specimens annealed at 1000 °C, 1050 °C, and 1150 °C are shown in Figure 9.

Figure 8. Curves of current density and temperature for specimens annealed at different temperatures in 1 M NaCl solution at an applied potential of 250 mV (SCE).

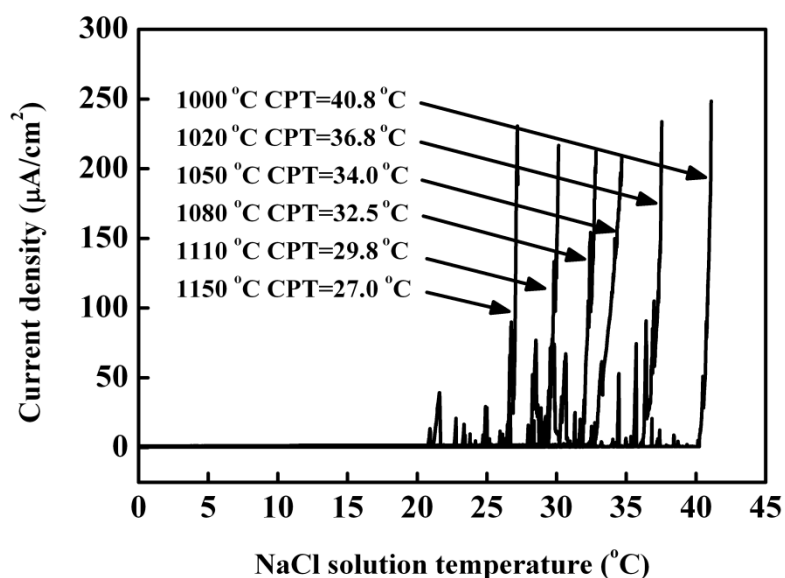
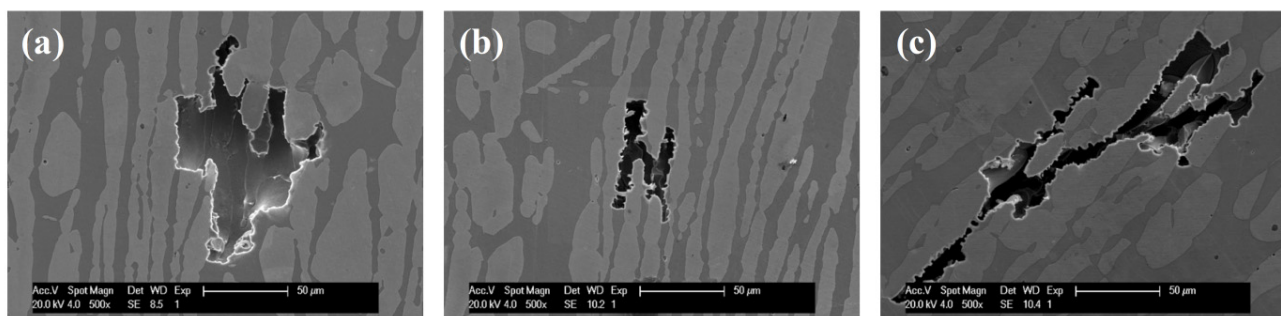


Figure 9. SEM morphologies of pittings formed on specimens annealed at different temperature for 30 min after the CPT test. (a) 1000 °C; (b) 1050 °C; (c) 1150 °C.

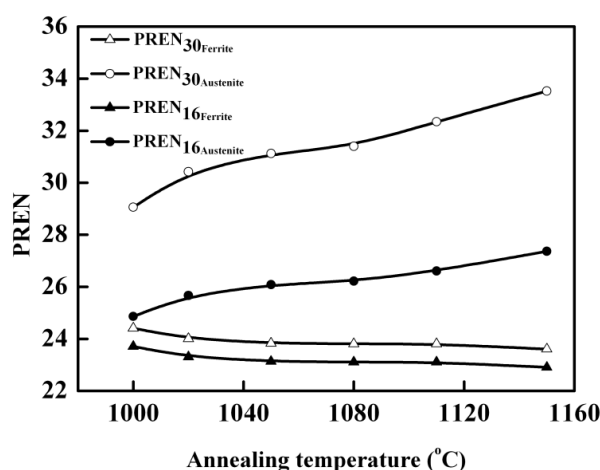


The resistance to pitting corrosion in duplex stainless steels was found to be strongly dependent on the chemical composition. It was known that the pitting resistance equivalent number of single phase could be used to evaluate the corrosion resistance of duplex stainless steels quickly. The empirical formula of pitting resistance equivalent number was defined by the following equation:

$$\text{PREN}_{16-30} = \text{wt\% Cr} + 3.3 \text{ wt\% Mo} + 16-30 \text{ wt\% N} \quad (1)$$

Different subscript varying in this formula indicated the different nitrogen coefficient [28–30]. The alloy (or phase) with higher pitting resistance equivalent number would exhibit better pitting corrosion resistance. Both the $PREN_{16}$ and $PREN_{30}$ of ferrite and austenite were calculated and listed in Table 2. Based on this formula, as the annealing temperature increased, the pitting resistance equivalent number of ferrite phase decreased while that of austenite phase increased. Figure 10 showed the pitting resistance equivalent number of single phase as function of annealing temperature. Such results were caused by the change of chemical composition of each phase corresponding to the variation of annealing temperature [31–33]. It has been reported that the pitting resistance of duplex stainless steels was determined by the weaker phase not the entire alloy [7,34]. For this novel lean duplex stainless steel, when the specimens were annealed at the temperature 1000 °C, both $PREN_{16}$ and $PREN_{30}$ differences between austenite and ferrite reached the lowest, which meant the two phases had similar pitting resistance at 1000 °C. Therefore, the pitting was propagated at both phases, shown in Figure 9a. However, the difference of $PREN_{16}$ between two phases was lower than that of $PREN_{30}$, indicating that it was better to use $PREN_{16}$ to explain the pitting corrosion behavior, which was in good agreement with the reported literature: 16 was the most frequently used subscript [2]. When the annealing temperature exceeded 1000 °C, the pitting resistance equivalent number of austenite phase was much higher than that of ferrite phase, and pitting mainly occurred in the ferrite phase. The pitting morphologies of specimen annealed at 1150 °C showed that pits were located mainly at ferrite areas, as shown in Figure 9c, indicating that the ferrite phase was much weaker than austenite phase. It could be found that the stable pitting morphologies of the specimens after CPT tests were fairly consistent with the pitting resistance equivalent number of the weaker phase for this new lean duplex stainless steel. It also could be obtained that the CPT reflected the pitting corrosion resistance of the weaker phase and that the pitting corrosion resistance of duplex stainless was determined by the weaker phase not the entire alloy.

Figure 10. PREN for each phase of specimens with different annealing temperatures for 30 min.



3.4. MFM and SKPFM Results

Figure 11 showed the microstructure of specimens after annealing treatment at 1000, 1050 and 1150 °C for 30 min using MFM and SKPFM. Figure 11a₁–a₃ respectively displayed the MFM images of the specimens annealed at 1000, 1050 and 1150 °C with 80 μm × 80 μm, where striped

ferromagnetic ferrite domain embedded in the paramagnetic austenite. Figure 11b₁–b₃ respectively revealed the SKPFM images of the same area with 80 μm × 80 μm. Figure 11c₁–c₃ demonstrated the Volta potential differences between the ferrite and austenite of specimens. The ferromagnetic ferrite had a lower Volta potential than the austenite. This was the same propensity as seen in the previous work [35–37]. The Volta potential difference between ferrite and austenite increased as the increase of annealing temperature. As shown in Table 4, the average potential difference between ferrite and austenite for the specimens annealed at 1000 °C, 1050 °C, 1150 °C were about 37.5 mV, 50 mV, and 75 mV. The highest value of Volta potential difference was obtained from specimen annealed at 1150 °C, and the lowest was from the specimen annealed at 1000 °C. A linear relationship between the Volta potential measured by SKPFM and corrosion potential has been reported [38–42]. It was reported that the possible galvanic interactions between the ferrite and austenite phases had been obtained by SKPFM technique [43]. In this paper, the ferrite had a lower Volta potential in this novel lean duplex stainless steel using SKPFM, which was in good agreement with the results in potentiostatic measurement (CPT) that pitting corrosion was found to be preferentially occurred in ferrite phase and the ferrite was a weaker phase. Compared with SKPFM technique, CPT measurement was performed at an applied potential. It couldn't be explained by galvanic interactions. However, a conclusion might be obtained that the pitting corrosion tendency of ferrite increased when applying a static potential. In addition, the Volta potential difference between ferrite and austenite was well consistent with the difference between $PREN_{\text{Ferrite}}$ and $PREN_{\text{Austenite}}$, which could be explained by that the elements of Cr, Mo, and N should have certain influences on the Volta potential [35].

Figure 11. (a₁–a₃) MFM and (b₁–b₃) SKPFM images of specimens respectively annealed at 1000 °C, 1050 °C and 1150 °C for 30 min; (c₁–c₃) volta potential difference profile of a line as showed in (b₁–b₃).

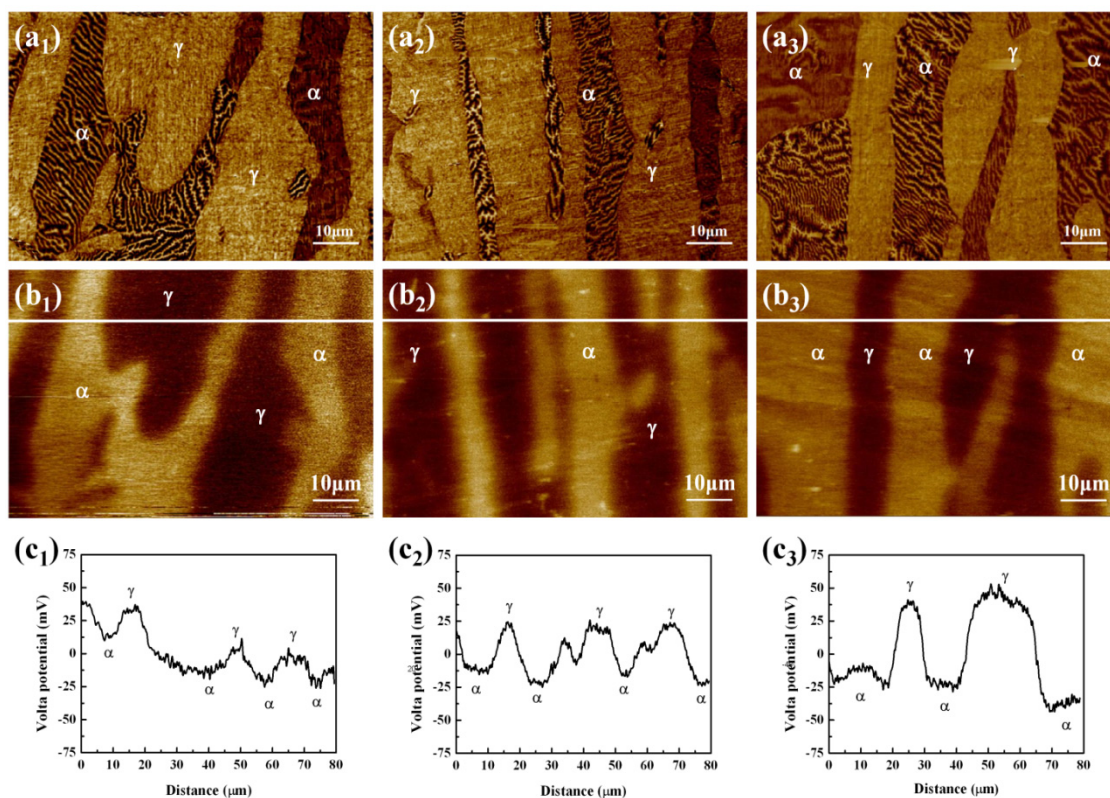


Table 4. The Volta potential difference between ferrite and austenite phase for the specimens annealed at 1000, 1050, and 1150 °C.

Annealing temperature (°C)	Average Volta potential difference _{Ferrite-Austenite} (mV)
1000	37.5
1050	50
1150	75

4. Conclusions

A novel lean duplex stainless steel 20Cr-2Ni-3Mn-0.17N-0.31Mo has been developed with higher elongation at break and better pitting corrosion resistance than UNS S32101. It has a great potential to be the promising replacement of S32101 in the advantage of improved properties. In order to expand the application of this new developed duplex steel, it is of great importance to obtain the suitable mechanical properties and good corrosion resistance. Thus, the effect of annealing temperature on the microstructure, mechanical properties and corrosion behavior of this novel lean duplex stainless steel has been characterized by microscope, mechanical test and electrochemical technique. Based on the experimental results, it is discovered that the best mechanical properties and pitting corrosion resistance of this newly developed DSS can be obtained at annealing temperature 1000 °C, which should be of great help in the industrial production. The main conclusions are as follows.

- (1) The volume fraction of austenite decreased continuously and the ferrite increased with the annealing temperature increasing from 1000 to 1150 °C.
- (2) The tensile strength and yield strength decreased with the increase of annealing temperature, which could be explained by the grain size and solid solution strengthening effects of alloying elements.
- (3) The elongation at break reached the maximum of 52.7% after annealing at 1050 °C due to martensite transformation associated with TRIP effect.
- (4) The critical pitting temperature decreased with increasing of annealing temperature. The localized pitting attack preferentially occurred at ferrite phase. The pitting corrosion behavior in chloride solutions could be explained by redistribution of main alloying elements, such as chromium, molybdenum and nitrogen in two phases, resulting in the change of $PREN_{16}$ of ferrite and austenite phases.
- (5) Ferrite had a lower Volta potential than austenite phase. The Volta potential difference between ferrite and austenite increased as the increase of annealing temperature. The Volta potential difference between ferrite and austenite was in good conformity with the difference between $PREN_{Ferrite}$ and $PREN_{Austenite}$.

Acknowledgments

The financial support from the National Natural Science Fund of China (Grants No. 51371053, 51131008 and 51134010), the National Key Technology R&D Program (2012BAE04B00), and the Discipline Development Fund of Science and Technology on Surface Physics and Chemistry Laboratory (ZDXKFZ201213) are gratefully acknowledged.

Author Contributions

The specimens were supported by Laizhu Jiang. The experiments were carried out by Yanjun Guo and Jincheng Hu, morphology characterization was performed by Tianwei Liu and Yanping Wu, the experimental scheme was framed by Jin Li. The manuscript was composed by Yanjun Guo and revised by Jincheng Hu.

Conflicts of Interest

The authors declare no conflicts of interest.

References

1. Nilsson, J.O. Super duplex stainless-steels. *Mater. Sci. Technol.* **1992**, *8*, 685–700.
2. Chen, T.H.; Yang, J.R. Effects of solution treatment and continuous cooling on sigma-phase precipitation in a 2205 duplex stainless steel. *Mater. Sci. Eng. A* **2001**, *311*, 28–41.
3. He, H.; Zhang, T.; Zhao, C.Z.; Hou, K.; Meng, G.Z.; Shao, Y.W.; Wang, F.H. Effect of alternating voltage passivation on the corrosion resistance of duplex stainless steel. *J. Appl. Electrochem.* **2009**, *39*, 737–745.
4. Lee, K.M.; Cho, H.S.; Choi, D.C. Effect of isothermal treatment of SAF 2205 duplex stainless steel on migration of delta/gamma interface boundary and growth of austenite. *J. Alloys Compd.* **1999**, *285*, 156–161.
5. Nilsson, J.O.; Wilson, A. Influence of isothermal phase-transformations on toughness and pitting corrosion of super duplex stainless-steel SAF-2507. *Mater. Sci. Technol.* **1993**, *9*, 545–554.
6. Sato, Y.S.; Nelson, T.W.; Sterling, C.J.; Steel, R.J.; Pettersson, C.O. Microstructure and mechanical properties of friction stir welded SAF 2507 super duplex stainless steel. *Mater. Sci. Eng. A* **2005**, *397*, 376–384.
7. Weber, L.; Uggowitzer, P.J. Partitioning of chromium and molybdenum in super duplex stainless steels with respect to nitrogen and nickel content. *Mater. Sci. Eng. A* **1998**, *242*, 222–229.
8. Alfonsso, E. Lean Duplex—The First Decade of Service Experience. In Proceedings of the 8th Duplex Stainless Steels Conference, Beaune, France, 13–15 October **2010**.
9. Zhang, W.; Jiang, L.Z.; Hu, J.C.; Song, H.M. Effect of ageing on precipitation and impact energy of 2101 economical duplex stainless steel. *Mater. Charact.* **2009**, *60*, 50–55.
10. Zhang, L.H.; Zhang, W.; Jiang, Y.M.; Deng, B.; Sun, D.M.; Li, J. Influence of annealing treatment on the corrosion resistance of lean duplex stainless steel 2101. *Electrochim. Acta* **2009**, *54*, 5387–5392.
11. Sieurin, H.; Sandstrom, R.; Westin, E.M. Fracture toughness of the lean duplex stainless steel LDX 2101. *Metall. Mater. Trans. A* **2006**, *37A*, 2975–2981.
12. Zhang, L.H.; Jiang, Y.M.; Deng, B.; Zhang, W.; Xu, J.L.; Li, J. Effect of aging on the corrosion resistance of 2101 lean duplex stainless steel. *Mater. Charact.* **2009**, *60*, 1522–1528.
13. Zhang, W.; Hu, J.H. Effect of annealing temperature on transformation induced plasticity effect of a lean duplex stainless steel. *Mater. Charact.* **2013**, *79*, 37–42.

14. Herrera, C.; Ponge, D.; Raabe, D. Design of a novel Mn-based 1 GPa duplex stainless TRIP steel with 60% ductility by a reduction of austenite stability. *Acta Mater.* **2011**, *59*, 4653–4664.
15. Choi, J.Y.; Ji, J.H.; Hwang, S.W.; Park, K.T. Strain induced martensitic transformation of Fe-20Cr-5Mn-0.2Ni duplex stainless steel during cold rolling: Effects of nitrogen addition. *Mater. Sci. Eng. A* **2011**, *528*, 6012–6019.
16. Pohl, M.; Storz, O.; Glogowski, T. Effect of intermetallic precipitations on the properties of duplex stainless steel. *Mater. Charact.* **2007**, *58*, 65–71.
17. Deng, B.; Wang, Z.Y.; Jiang, Y.M.; Sun, T.; Xu, J.L.; Li, J. Effect of thermal cycles on the corrosion and mechanical properties of UNS S31803 duplex stainless steel. *Corros. Sci.* **2009**, *51*, 2969–2975.
18. British Standards (BS) European Norm (EN) International Organization for Standardization (ISO) 6892-1:2009, “Metallic materials Tensile testing; Part 1: Method of test at ambient temperature”, European Committee for Standardization, Brüssel, **2009**.
19. American Society for Testing and Materials (ASTM) Standard G150-99. Standard Test Method for Electrochemical Critical Pitting Temperature Testing of Stainless Steels, Annual Book of ASTM Standards; ASTM International: West Conshohocken, PA, USA, 2010.
20. Tan, H.; Jiang, Y.M.; Deng, B.; Sun, T.; Xu, J.L.; Li, J. Effect of annealing temperature on the pitting corrosion resistance of super duplex stainless steel UNS S32750. *Mater. Charact.* **2009**, *60*, 1049–1054.
21. GarfíasMesias, L.F.; Sykes, J.M.; Tuck, C.D.S. The effect of phase compositions on the pitting corrosion of 25 Cr duplex stainless steel in chloride solutions. *Corros. Sci.* **1996**, *38*, 1319–1330.
22. Nonnenmacher, M.; Oboyle, M.P.; Wickramasinghe, H.K. Kelvin probe force microscopy. *Appl. Phys. Lett.* **1991**, *58*, 2921–2923.
23. Rohwerder, M.; Turcu, F. High-resolution Kelvin probe microscopy in corrosion science: Scanning Kelvin probe force microscopy (SKPFM) versus classical scanning Kelvin probe (SKP). *Electrochim. Acta* **2007**, *53*, 290–299.
24. Yousefieh, M.; Shamanian, M.; Saatchi, A. Influence of step annealing temperature on the microstructure and pitting corrosion resistance of SDSS UNS S32760 welds. *J. Mater. Eng. Perform.* **2011**, *20*, 1678–1683.
25. Offerman, S.E.; van Dijk, N.H.; Sietsma, J.; Grigull, S.; Lauridsen, E.M.; Margulies, L.; Poulsen, H.F.; Rekveldt, M.T.; van der Zwaag, S. Grain nucleation and growth during phase transformations. *Science* **2002**, *298*, 1003–1005.
26. Badji, R.; Bacroix, B.; Bouabdallah, M. Texture, microstructure and anisotropic properties in annealed 2205 duplex stainless steel welds. *Mater. Charact.* **2011**, *62*, 833–843.
27. Zhang, X.D.; Hansen, N.; Gao, Y.K.; Huang, X.X. Hall-Petch and dislocation strengthening in graded nanostructured steel. *Acta Mater.* **2012**, *60*, 5933–5943.
28. Merello, R.; Botana, F.J.; Botella, J.; Matres, M.V.; Marcos, M. Influence of chemical composition on the pitting corrosion resistance of non-standard low-Ni high-Mn-N duplex stainless steels. *Corros. Sci.* **2003**, *45*, 909–921.
29. Bae, S.H.; Lee, H.W. Effect of Mo contents on corrosion behaviors of welded duplex stainless steel. *Met. Mater. Int.* **2013**, *19*, 563–569.

30. Munoz, A.I.; Anton, J.G.; Nuevalos, S.L.; Guinon, J.L.; Herranz, V.N. Corrosion studies of austenitic and duplex stainless steels in aqueous lithium bromide solution at different temperatures. *Corros. Sci.* **2004**, *46*, 2955–2974.
31. Zhong, C.; Liu, F.; Wu, Y.T.; Le, J.J.; Liu, L.; He, M.F.; Zhu, J.C.; Hu, W.B. Protective diffusion coatings on magnesium alloys: A review of recent developments. *J. Alloys Compd.* **2012**, *520*, 11–21.
32. Zhong, C.; He, M.F.; Liu, L.; Wu, Y.T.; Chen, Y.J.; Deng, Y.D.; Shen, B.; Hu, W.B. Lower temperature fabrication of continuous intermetallic coatings on AZ91D magnesium alloy in molten salts. *J. Alloys Compd.* **2010**, *504*, 377–381.
33. Le, J.J.; Liu, L.; Liu, F.; Deng, Y.D.; Zhong, C.; Hu, W.B. Interdiffusion kinetics of the intermetallic coatings on AZ91D magnesium alloy formed in molten salts at lower temperatures. *J. Alloys Compd.* **2014**, *610*, 173–179.
34. Mori, G.; Bauernfeind, D. Pitting and crevice corrosion of superaustenitic stainless steels. *Mater. Corros.* **2004**, *55*, 164–173.
35. Sathirachinda, N.; Pettersson, R.; Pan, J.S. Depletion effects at phase boundaries in 2205 duplex stainless steel characterized with SKPFM and TEM/EDS. *Corros. Sci.* **2009**, *51*, 1850–1860.
36. Guo, L.Q.; Li, M.; Shi, X.L.; Yan, Y.; Li, X.Y.; Qiao, L.J. Effect of annealing temperature on the corrosion behavior of duplex stainless steel studied by *in situ* techniques. *Corros. Sci.* **2011**, *53*, 3733–3741.
37. Sathirachinda, N.; Gubner, R.; Pan, J.; Kivisakk, U. Characterization of phases in duplex stainless steel by magnetic force microscopy/scanning kelvin probe force microscopy. *Electrochem. Solid State Lett.* **2008**, *11*, C41–C45.
38. Stratmann, M. The investigation of the corrosion properties of metals, covered with adsorbed electrolyte layers—A new experimental technique. *Corros. Sci.* **1987**, *27*, 869–872.
39. Stratmann, M.; Streckel, H. On the atmospheric corrosion of metals which are covered with thin electrolyte layers. 1. Verification of the experimental technique. *Corros. Sci.* **1990**, *30*, 681–696.
40. Yee, S.G.; Oriani, R.A.; Stratmann, M. Application of a kelvin microprobe to the corrosion of metals in humid atmospheres. *J. Electrochem. Soc.* **1991**, *138*, 55–61.
41. Schmutz, P.; Frankel, G.S. Characterization of AA2024-T3 by scanning Kelvin probe force microscopy. *J. Electrochem. Soc.* **1998**, *145*, 2285–2295.
42. Guillaumin, V.; Schmutz, P.; Frankel, G.S. Characterization of corrosion interfaces by the scanning Kelvin probe force microscopy technique. *J. Electrochem. Soc.* **2001**, *148*, B163–B173.
43. Femenia, M.; Canalias, C.; Pan, J.; Leygraf, C. Scanning Kelvin probe force microscopy and magnetic force microscopy for characterization of duplex stainless steels. *J. Electrochem. Soc.* **2003**, *150*, B274–B281.